

doi:10.11835/j.issn.1674-4764.2013.04.016

移动荷载作用下加筋路堤和轨道系统的三维动力响应

刘飞禹, 杨风云

(上海大学土木工程系, 上海 200072)

摘要:用解析法研究了加筋路堤上轨道系统在移动荷载作用下的三维动力响应问题。基于 Biot 多孔弹性介质的波动理论,建立了加筋路堤-轨道系统分析模型。将钢轨简化为无限长弹性 Euler 梁,将枕木简化为连续质量块,将加筋路堤作为一横观各向同性层来考虑,将下卧土体考虑为由 Biot 波动方程描述的饱和半空间。联立轨道系统、加筋路堤和下卧土体的动力方程,在 Fourier 变换域内求解荷载作用下钢轨位移和土体位移的表达式,将求得的表达式进行 Fourier 逆变换得到其在时域里的表达式。研究了列车移动速度、加筋路堤层的厚度、荷载幅值大小和加筋率等对路堤及轨道系统动力响应的影响。计算结果表明,钢轨竖向变形随着速度的增大呈现先增大后减小的趋势;加筋路堤上的钢轨竖向变形显著小于同厚度下未加筋路堤上的钢轨竖向变形;钢轨竖向变形随着荷载幅值的增大而增大;随着加筋率的增大而减小。

关键词:移动荷载;加筋路堤;轨道系统;动力响应

中图分类号:TU411 **文献标志码:**A **文章编号:**1674-4764(2013)04-0101-08

3-D Dynamic Response of Reinforced Embankment and Track System Subjected to Moving Traffic Load

Liu Feiyu, Yang Fengyun

(Department of Civil Engineering, Shanghai University, Shanghai 200072, P. R. China)

Abstract: An analytic method was used to study the dynamic response of track system on reinforced embankment subjected to moving traffic load. Based on Biot's dynamic poro-elastic theory, dynamic analytical model of track system and reinforced embankment was established. The rails were described as an infinitely long Euler beam subjected to moving axle loads and sleepers were represented by continuous mass. Reinforced embankment embedded between track system and poro-elastic subsoil was modeled as a transversely isotropic layer. Subsoil was fully saturated poroelastic medium governed by the Biot's theory. Using the Fourier transform, the governing equations were then solved analytically in the frequency-wave-number domain. The time domain responses were obtained by the inverse Fourier transform computation. The influences of the train velocity, thickness of reinforced layer, load amplitude and reinforcement's ratio on the displacement responses of rails were carefully investigated. Computed results show that the vertical displacement of rails increases with the increase of load speed initially and decreases later. The displacement of rails with reinforced embankment is less than the ones without reinforced embankment. The displacement of rails increases with the increase of load amplitude and decreases with the increase of reinforcement's ratio.

Key words: moving load; reinforced embankment; track system; dynamic response

收稿日期:2013-01-08

基金项目:国家自然科学基金(50808119)

作者简介:刘飞禹(1976-),男,博士,副教授,主要从事加筋土的动力响应研究,(E-mail)flyingrainliu@gmail.com.

近年来,加筋路堤由于其良好的工程性能和经济性,受到了广泛关注,许多学者对路堤加筋问题进行了研究。Wang 等^[1]采用离心试验的方法研究了地震荷载作用下土工合成材料加筋路堤的特性。Nazzal 等^[2]采用有限元方法研究了基层内放置土工合成材料对柔性路面结构响应的影响。Kwon 等^[3]采用一种机械的反应模型验证了土工格栅能增强柔性路面的刚度。Huang 等^[4]采用离心分离模型试验和二维有限元的方法,比较了加筋和不加筋路堤上道路响应。Malleshwari 等^[5]研究了条形荷载作用下加筋地基上。无限长梁的动力响应,但他只考虑二维作用下的情况,并且没有考虑孔隙水的影响。刘飞禹等^[6]研究了二维情况下匀速移动条形线荷载作用下的加筋道路体系的动力响应问题。Saad 等^[7]采用三维有限元的方法对室内加筋路堤模型在循环荷载作用下的特性进行了分析。

另一方面,随着高速铁路和公路的快速发展,移动荷载作用下轨道系统的动力响应问题越来越受到重视^[8-11]。Sun 等^[12]研究了层状地基土体上轨道系统在列车荷载作用下的动力响应问题。Xu 等^[13-14]分别研究了移动荷载作用下饱和成层土体的动力响应以及下卧成层饱和土体上 Euler 梁的动力响应问题。但是,移动荷载作用下加筋路堤上轨道系统的动力响应问题还未见有人研究。

本文采用解析法研究了移动荷载作用下,下卧饱和土体上加筋路堤及其上轨道系统的动力响应问题,着重研究了列车移动速度、加筋路堤层的厚度、加筋率等对路堤及轨道系统动力响应的影响。

1 控制方程及求解

轨道系统模型如图 1 所示,将钢轨简化为无限长弹性 Euler 梁,将枕木简化为连续质量块,同时考虑由 Cosserat 模型描述的道砟层;加筋路堤一般采用土工格栅、土工织物等与土体分层填筑,由于每层相互平行且间距相等,所以将加筋路堤看作一横观各向同性层来考虑;将下卧土体考虑为由 Biot 波动方程描述的饱和半空间。

1.1 多孔饱和半空间土体控制方程及求解

根据 Biot 理论^[15],饱和孔隙介质及孔隙流体的动量守恒方程分别为

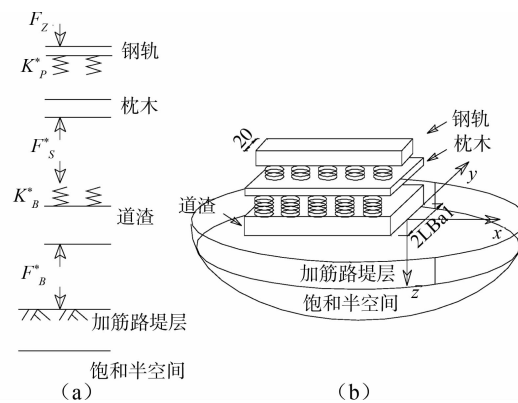


图 1 轨道系统和加筋路堤模型

$$\mu u_{i,jj} + (\lambda + \alpha^2 M + \mu) u_{j,ii} - \alpha M \tau_{j,ii} = (\rho \ddot{u}_i + \rho_f \ddot{w}_i) \quad (1)$$

$$\alpha M u_{j,ji} + M \tau_{j,ji} = \rho_f \ddot{u}_i + m \ddot{w}_i + b \dot{w}_i \quad (2)$$

式中: $u_i, \tau_{ij} (i = x, y, z)$ 分别为土骨架沿 x, y, z 方向的位移分量和流体在 x, y, z 方向相对于土骨架的位移分量; λ, μ 均为 Lamé 常数; α, M 为表征土颗粒和孔隙流体压缩性的常数; b 为流体的动力黏滞系数与土体的渗透系数的比值; $\rho = n \rho_f + (1 - n) \rho_s$, 其中 ρ_f 为流体的质量密度, ρ_s 为土体骨架的质量密度, n 为土体的孔隙率; $m = \rho_f / n$ 。

土体的应力应变关系及土体的渗流连续方程分别为:

$$\sigma_{ij} = \lambda \theta \delta_{ij} + \mu (u_{i,j} + u_{j,i}) - \alpha \delta_{ij} p_f \quad (3)$$

$$-\dot{p}_f = M \dot{w}_{i,i} + \alpha M \dot{u}_{i,i} \quad (4)$$

式中: σ_{ij} 为土体骨架总应力分量; p_f 为孔隙水压力。本文采用无量纲变量,用上标 * 来表示无量纲变量。定义如下: $p_f^* = p_f / \mu$;

$$u_x^* = u_x / a; u_y^* = u_y / a; u_z^* = u_z / a;$$

$$\sigma_z^* = \sigma_z / \mu; \tau_{xx}^* = \tau_{xx} / \mu; \tau_{yz}^* = \tau_{yz} / \mu$$

引入无量纲坐标: $x^* = x / a; y^* = y / a; z^* = z / a$, 其中 a 为 Euler 梁宽度的一半。

对无量纲时间 τ 的 Fourier 变换以及逆变换定义如下:

$$\left. \begin{aligned} \tilde{f}(x^*, y^*, z^*, a_0) &= \\ \int_{-\infty}^{+\infty} f(x^*, y^*, z^*, \tau) e^{-ia_0 \tau} d\tau \\ f(x^*, y^*, z^*, \tau) &= \\ \frac{1}{2\pi} \int_{-\infty}^{+\infty} \tilde{f}(x^*, y^*, z^*, a_0) e^{ia_0 \tau} da_0 \end{aligned} \right\} \quad (5)$$

式中: $\tau = (t/a) \sqrt{\mu/\rho}$ 为无量纲时间; a_0 为 Fourier 变换参数。

无量纲坐标 x^* 及 y^* 的双重 Fourier 变换及逆变换如下:

$$\left. \begin{aligned} \bar{\bar{f}}(\epsilon, \eta, z^*, a_0) &= \int_{-\infty}^{+\infty} \int_{-\infty}^{+\infty} \tilde{f}(x^*, y^*, z^*, a_0) e^{-i(\epsilon x^* + \eta y^*)} dx^* dy^* \\ \tilde{f}(x^*, y^*, z^*, a_0) &= \frac{1}{4\pi^2} \int_{-\infty}^{+\infty} \int_{-\infty}^{+\infty} \bar{\bar{f}}(\epsilon, \eta, z^*, a_0) e^{i(\epsilon x^* + \eta y^*)} d\epsilon d\eta \end{aligned} \right\} \quad (6)$$

对方程(1)~(4)进行三重 Fourier 变换,把偏微分方程变为常微分方程,解常微分方程得到:

$$\bar{\bar{p}}_f^*(\epsilon, \eta, z^*, a_0) = A(\epsilon, \eta, a_0) e^{-\gamma_1 z^*} + B(\epsilon, \eta, a_0) e^{-\gamma_2 z^*} \quad (7)$$

$$\bar{\bar{u}}_z^*(\epsilon, \eta, z^*, a_0) = \gamma_1 a_1 A e^{-\gamma_1 z^*} + \gamma_2 a_2 B e^{-\gamma_2 z^*} + C e^{-\gamma_3 z^*} \quad (8)$$

$$\bar{\bar{u}}_y^*(\epsilon, \eta, z^*, a_0) = -i\eta(a_1 A e^{-\gamma_1 z^*} + a_2 B e^{-\gamma_2 z^*}) + iD e^{-\gamma_3 z^*} \quad (9)$$

$$\bar{\bar{u}}_x^*(\epsilon, \eta, z^*, a_0) = -\frac{i}{\epsilon} \{ [\chi_1 + (\epsilon^2 - L_1^2) a_1] \cdot A e^{-\gamma_1 z^*} + [\chi_2 + (\epsilon^2 - L_2^2) a_2] B e^{-\gamma_2 z^*} + (C\gamma_3 + D\eta) e^{-\gamma_3 z^*} \} \quad (10)$$

式中:由于当 $z \rightarrow \infty$ 时,土体的动力响应为零,对于 $\gamma_i (i = 1, 2, 3)$, 必须有 $\text{Re}(\gamma_i) \geq 0$; A, B, C, D 为 ϵ, η, a_0 的函数,由边界条件确定;

$$\gamma_i = \sqrt{\epsilon^2 + \eta^2 - L_i^2} \quad (i = 1, 2)$$

$$\gamma_3 = \sqrt{\epsilon^2 + \eta^2 - S^2}$$

$$\chi_i = \frac{\partial M^* L_i^2 - \rho^* a_0^2}{\rho^* a_0^2 (\alpha - \partial) M^*} \quad (i = 1, 2)$$

$$a_i = \frac{\lambda^* \chi_i + \chi_i - \alpha + \partial}{S^2 - L_i^2} \quad (i = 1, 2)$$

$$L_1^2 = \frac{\beta_1 + \sqrt{\beta_1^2 - 4\beta_2}}{2}$$

$$L_2^2 = \frac{\beta_1 - \sqrt{\beta_1^2 - 4\beta_2}}{2}$$

$$S = (1 - \rho^* \partial) a_0^2$$

上述式中的 L_1, L_2, S 分别为对应于第一、二类 P 波及 S 波的无量纲波数。利用物理方程求得:

$$\bar{\bar{\sigma}}_{0xz}^* = g_3 A e^{-\gamma_1 z^*} + g_4 B e^{-\gamma_2 z^*} - 2\gamma_3 C e^{-\gamma_3 z^*} \quad (11)$$

$$\bar{\bar{\tau}}_{0xz}^* = i \left[\frac{\gamma_1 g_1}{\epsilon} A e^{-\gamma_1 z^*} + \frac{\gamma_2 g_2}{\epsilon} B e^{-\gamma_2 z^*} + \frac{C(\gamma_3^2 + \epsilon^2) + D\gamma_3 \eta}{\epsilon} e^{-\gamma_3 z^*} \right] \quad (12)$$

$$\bar{\bar{\tau}}_{0yz}^* = i [2\eta\gamma_1 a_1 A e^{-\gamma_1 z^*} + 2\eta\gamma_2 a_2 B e^{-\gamma_2 z^*} + (C\eta - D\gamma_3) e^{-\gamma_3 z^*}] \quad (13)$$

式中: $g_1 = \chi_1 + (2\epsilon^2 - L_1^2) a_1$

$$g_2 = \chi_2 + (2\epsilon^2 - L_2^2) a_2$$

$$g_3 = \lambda^* \chi_1 - 2\gamma_1^2 a_1 - \alpha$$

$$g_4 = \lambda^* \chi_2 - 2\gamma_2^2 a_2 - \alpha$$

1.2 加筋路堤的控制方程

将加筋路堤看成宏观上的横观各向同性体,加筋复合土体横观各向同性参数的表达式如下,具体推导过程可参见文献[16]。

$$E_h = \frac{1}{1 + \eta} \left[\frac{(\Omega^r + \Omega^s)^2 - (\mu^r \Omega^r + \mu^s \Omega^s)^2}{\Omega^r + \Omega^s} \right] \quad (14)$$

$$\mu_{hh} = \frac{\mu^r \Omega^r + \mu^s \Omega^s}{\Omega^r + \Omega^s} \quad (15)$$

$$\mu_{hv} = \frac{(1 - \mu^r) \Omega^r + (1 - \mu^s) \Omega^s}{(1 + \eta)(\Omega^r + \Omega^s)} (\Psi^r + \Psi^s) \quad (16)$$

$$\frac{1}{E_v} = \frac{1}{1 + \eta} \left\{ \frac{\eta^2}{\Omega^r} + \frac{1}{\Omega^s} + \left[\frac{2}{(1 + \mu^r) \Omega^r + (1 + \mu^s) \Omega^s} - \frac{1}{\Omega^r + \Omega^s} \right] (\Psi^r + \Psi^s)^2 \right\} \quad (17)$$

$$\frac{1}{G_{hv}} = \frac{1}{1 + \eta} \left(\frac{\eta^2}{\Omega^r} + \frac{1}{\Omega^s} \right) + \frac{(1 + \mu_{hh})^2}{E_h} \quad (18)$$

其中: E_h, E_v 分别为加筋复合土体水平和垂直方向的弹性模量; G_{hv} 为加筋复合土体水平方向剪切模量; μ_{hh} 为水平方向应力在水平方向引起侧向变形的泊松比; μ_{hv} 为水平方向应力在垂直方向引起侧向变形的泊松比; $\Omega^r = \eta E^r / [1 - (\mu^r)^2], \Omega^s = E^s / [1 - (\mu^s)^2]$,

$$\Psi^r = \eta \mu^r / (1 - \mu^r), \Psi^s = \mu^s / (1 - \mu^s)。$$

复合土体的加筋率 η 表示为^[17]:

$$\eta = \frac{V^r}{V^s} = \frac{A^r}{A^s} = \frac{S^r}{S^s} \quad (19)$$

式中: V^r, A^r, S^r 分别为加筋单元层中加筋材料的体积、横截面面积和横截面的厚度; V^s, A^s, S^s 分别为加筋单元层中土体的体积、横截面面积和横截面的厚度。

根据土介质中波的传播理论,横观各向同性加筋路堤的控制方程为:

$$\left. \begin{aligned} C_{11} \frac{\partial^2 u}{\partial x^2} + C_{66} \frac{\partial^2 u}{\partial y^2} + C_{44} \frac{\partial^2 u}{\partial z^2} + (C_{12} + C_{66}) \frac{\partial^2 v}{\partial x \partial y} + (C_{13} + C_{44}) \frac{\partial^2 w}{\partial x \partial z} &= \rho \ddot{u} \\ (C_{12} + C_{66}) \frac{\partial^2 u}{\partial x \partial y} + C_{66} \frac{\partial^2 v}{\partial x^2} + C_{11} \frac{\partial^2 v}{\partial y^2} + C_{44} \frac{\partial^2 v}{\partial z^2} + (C_{13} + C_{44}) \frac{\partial^2 w}{\partial y \partial z} &= \rho \ddot{v} \\ (C_{13} + C_{44}) \frac{\partial^2 u}{\partial x \partial z} + (C_{13} + C_{44}) \frac{\partial^2 v}{\partial y \partial z} + C_{44} \frac{\partial^2 w}{\partial x^2} + C_{44} \frac{\partial^2 w}{\partial y^2} + C_{33} \frac{\partial^2 w}{\partial z^2} &= \rho \ddot{w} \end{aligned} \right\} \quad (20)$$

式中:其中 $C_{11}, C_{12}, C_{13}, C_{33}, C_{44}, C_{66}$ 为横观各向同性弹性常数,即:

$$\begin{aligned} C_{11} &= \frac{2G_h(1 - \mu_{hv}\mu_{vh})}{1 - \mu_{hh} - 2\mu_{vh}\mu_{hv}}, \\ C_{12} &= \frac{2G_h(1 - \mu_{hh}^2)}{1 - \mu_{hh} - 2\mu_{vh}\mu_{hv}}, \\ C_{13} &= \frac{2G_h(1 + \mu_{hh})\mu_{vh}}{1 - \mu_{hh} - 2\mu_{vh}\mu_{hv}}, \\ C_{33} &= \frac{2G_h(1 - \mu_{hh}^2)\mu_{vh}}{\mu_{hh}(1 - \mu_{hh} - 2\mu_{vh}\mu_{hv})}, \\ C_{44} &= G_v, C_{66} = \frac{1}{2}(C_{11} - C_{12}) \end{aligned}$$

G_{hv} 为土体水平方向剪切模量; μ_{vh} 竖直方向应力在水平方向引起侧向变形的泊松比。

定义对无量纲时间 τ 的 Fourier 变换如下:

$$\left. \begin{aligned} \tilde{\varphi}(x^*, y^*, z^*, \Omega) &= \int_{-\infty}^{+\infty} \varphi(x^*, y^*, z^*, \tau) e^{-i\Omega\tau} d\tau \\ \varphi(x^*, y^*, z^*, \tau) &= \frac{1}{2\pi} \int_{-\infty}^{+\infty} \tilde{\varphi}(x^*, y^*, z^*, \Omega) e^{i\Omega\tau} d\Omega \end{aligned} \right\} \quad (21)$$

定义对无量纲自变量 x^*, y^* 的 Fourier 变换及其逆变换如下:

$$\left. \begin{aligned} \tilde{f}(\varepsilon, \eta, z^*, \Omega) &= \int_{-\infty}^{+\infty} \int_{-\infty}^{+\infty} f(x^*, y^*, z^*, \Omega) e^{-i(\varepsilon x^* + \eta y^*)} dx^* dy^* \\ f(x^*, y^*, z^*, \Omega) &= \frac{1}{4\pi^2} \int_{-\infty}^{+\infty} \int_{-\infty}^{+\infty} \tilde{f}(\varepsilon, \eta, z^*, \Omega) e^{i(\varepsilon x^* + \eta y^*)} d\varepsilon d\eta \end{aligned} \right\} \quad (22)$$

将式(20)进行 Fourier 变换,可得如下表达式:

$$\left. \begin{aligned} a_1 \bar{u}^* + b_1 \frac{\partial^2 \bar{u}^*}{\partial z^{*2}} + c_1 \frac{\partial \bar{w}^*}{\partial z^*} + d_1 \bar{v}^* &= 0 \\ a_2 \bar{v}^* + b_2 \frac{\partial^2 \bar{v}^*}{\partial z^{*2}} + c_2 \frac{\partial \bar{w}^*}{\partial z^*} + d_2 \bar{u}^* &= 0 \\ a_3 \bar{w}^* + b_3 \frac{\partial^2 \bar{w}^*}{\partial z^{*2}} + c_3 \frac{\partial \bar{u}^*}{\partial z^*} + d_3 \frac{\partial \bar{v}^*}{\partial z^*} &= 0 \end{aligned} \right\} \quad (23)$$

式中:

$$\begin{aligned} L_1 &= -\Omega^2, x^* = x/a, y^* = y/a, z^* = z/a, \tau = (t/a) \sqrt{\mu/\rho} \\ a_1 &= C_{11}\xi^2 + C_{66}\eta^2 + L_1\rho, b_1 = -C_{44}, c_1 = -(C_{13} + C_{44})i\xi \\ d_1 &= (C_{12} + C_{66})\xi\eta, a_2 = C_{66}\xi^2 + C_{11}\eta^2 + L_1\rho, b_2 = -C_{44} \\ c_2 &= -(C_{13} + C_{44})i\eta, d_2 = (C_{12} + C_{66})\xi\eta, a_3 = \end{aligned}$$

$$\begin{aligned} -C_{44}(\xi^2 + \eta^2) - L_1\rho \\ b_3 = C_{33}, c_3 = (C_{13} + C_{44})i\xi, d_3 = (C_{13} + C_{44})i\eta \end{aligned}$$

式(23)解的基本形式为:

$$\begin{aligned} \bar{u}^* &= \sum_{k=1}^6 A_k e^{r_k z^*}, \bar{v}^* = \sum_{k=1}^6 B_k e^{r_k z^*}, \\ \bar{w}^* &= \sum_{k=1}^6 C_k e^{r_k z^*} \end{aligned} \quad (24)$$

将式(24)代入式(23),得:

$$\left. \begin{aligned} (a_1 + b_1 r^2)A + d_1 B + c_1 r C &= 0 \\ d_2 A + (a_2 + b_2 r^2)B + c_2 r C &= 0 \\ c_3 r A + d_3 r B + (a_3 + b_3 r^2)C &= 0 \end{aligned} \right\} \quad (25)$$

要使 A, B, C 有非零解,则式(25)的系数行列式的值必为零,即:

$$\begin{vmatrix} a_1 + b_1 r^2 & d_1 & c_1 r \\ d_2 & a_2 + b_2 r^2 & c_2 r \\ c_3 r & d_3 r & a_3 + b_3 r^2 \end{vmatrix} = 0 \quad (26)$$

设 r_k 为(26)的解,将 r_k 代入式(25)得 B_k, C_k 的表达式,即:

$$B_k = R_k A_k, C_k = M_k A_k \quad (27)$$

其中 R_k, M_k 的表达式如下:

$$\begin{aligned} R_k &= \frac{r_k[-c_1 d_2 + c_2(a_1 + b_1 r_k^2)]}{-c_2 d_1 r_k + c_1 r_k(a_2 + b_2 r_k^2)} \\ M_k &= \frac{d_1 d_2 - (a_1 + b_1 r_k^2)(a_2 + b_2 r_k^2)}{-c_2 d_1 r_k + c_1 r_k(a_2 + b_2 r_k^2)} \end{aligned}$$

为了满足半空间无限远处土体动力为零的辐射条件,忽略实部为正的 r_k , 则:

$$\begin{aligned} \bar{u}^* &= \sum_{k=1}^3 A_k e^{r_k z^*}, \bar{v}^* = \sum_{k=1}^3 B_k e^{r_k z^*}, \\ \bar{w}^* &= \sum_{k=1}^3 C_k e^{r_k z^*} \end{aligned} \quad (28)$$

$$\frac{\partial \bar{u}^*}{\partial z} = \sum_{k=1}^3 r_k A_k e^{r_k z^*}, \frac{\partial \bar{v}^*}{\partial z} = \sum_{k=1}^3 r_k R_k A_k e^{r_k z^*},$$

$$\frac{\partial \bar{w}^*}{\partial z} = \sum_{k=1}^3 r_k M_k A_k e^{r_k z^*} \quad (29)$$

加筋路堤弹性介质中的应力-应变关系为:

$$\left. \begin{aligned} \sigma_z &= C_{13}\varepsilon_x + C_{13}\varepsilon_y + C_{33}\varepsilon_z \\ \tau_{xz} &= C_{44}\gamma_{xz} \\ \tau_{yz} &= C_{44}\gamma_{yz} \end{aligned} \right\} \quad (30)$$

由几何方程

$$\left. \begin{aligned} \gamma_{xz} &= \frac{\partial u_x}{\partial z} + \frac{\partial u_z}{\partial x} = \frac{\partial u}{\partial z} + \frac{\partial w}{\partial x} \\ \gamma_{yz} &= \frac{\partial u_z}{\partial y} + \frac{\partial u_y}{\partial z} = \frac{\partial v}{\partial z} + \frac{\partial w}{\partial y} \\ \varepsilon_x &= \frac{\partial u_x}{\partial x} = \frac{\partial u}{\partial x} \\ \varepsilon_y &= \frac{\partial u_y}{\partial y} = \frac{\partial v}{\partial y} \\ \varepsilon_z &= \frac{\partial u_z}{\partial z} = \frac{\partial w}{\partial z} \end{aligned} \right\} \quad (31)$$

将(31)代入(30)中得:

$$\left. \begin{aligned} \sigma_z^* &= C_{13} \frac{\partial u^*}{\partial x^*} + C_{13} \frac{\partial v^*}{\partial y^*} + C_{33} \frac{\partial w^*}{\partial z^*} \\ \tau_{xz}^* &= C_{44} \left(\frac{\partial u^*}{\partial z^*} + \frac{\partial w^*}{\partial x^*} \right) \\ \tau_{yz}^* &= C_{44} \left(\frac{\partial v^*}{\partial z^*} + \frac{\partial w^*}{\partial y^*} \right) \end{aligned} \right\} \quad (32)$$

对(32)进行三重 Fourier 变换 $(x^*, y^*, \tau) \sim (\xi, \eta, \Omega)$, 可得:

$$\left. \begin{aligned} \bar{\sigma}_z^* &= i\xi C_{13} \bar{u}^* + i\eta C_{13} \bar{v}^* + C_{33} \frac{\partial \bar{w}^*}{\partial z^*} \\ \bar{\tau}_{xz}^* &= C_{44} \left(\frac{\partial \bar{u}^*}{\partial z^*} + i\xi \bar{w}^* \right) \\ \bar{\tau}_{yz}^* &= C_{44} \left(\frac{\partial \bar{v}^*}{\partial z^*} + i\eta \bar{w}^* \right) \end{aligned} \right\} \quad (33)$$

将式(29)代入(33)中得:

$$\left. \begin{aligned} \bar{\sigma}_z^* &= \sum_{k=1}^3 [C_{13} (i\xi + i\eta R_k) + C_{33} r_k M_k] A_k e^{r_k z^*} \\ \bar{\tau}_{xz}^* &= \sum_{k=1}^3 C_{44} (r_k + i\xi M_k) A_k e^{r_k z^*} \\ \bar{\tau}_{yz}^* &= \sum_{k=1}^3 C_{44} (r_k R_k + i\eta M_k) A_k e^{r_k z^*} \end{aligned} \right\} \quad (34)$$

引用空间辅助坐标 $x_t^* = x^* - c\tau$ 后,得加筋路堤的位移表达式:

$$\left. \begin{aligned} u^*(x_t^*, y^*, z^*) &= \frac{1}{4\pi^2} \int_{-\infty}^{+\infty} \int_{-\infty}^{+\infty} \left(\sum_{k=1}^3 A_k e^{r_k z^*} \right) e^{i(\xi x_t^* + \eta y^*)} d\xi d\eta \\ v^*(x_t^*, y^*, z^*) &= \frac{1}{4\pi^2} \int_{-\infty}^{+\infty} \int_{-\infty}^{+\infty} \left(\sum_{k=1}^3 R_k A_k e^{r_k z^*} \right) e^{i(\xi x_t^* + \eta y^*)} d\xi d\eta \\ w^*(x_t^*, y^*, z^*) &= \frac{1}{4\pi^2} \int_{-\infty}^{+\infty} \int_{-\infty}^{+\infty} \left(\sum_{k=1}^3 M_k A_k e^{r_k z^*} \right) e^{i(\xi x_t^* + \eta y^*)} d\xi d\eta \end{aligned} \right\} \quad (35)$$

1.3 利用边界条件求解

引入边界条件:

$$\sigma_{zz}^*(x^*, y^*, 0, \tau) = -\frac{1}{2a} \Pi(y^*) q_z^*(x^*, \tau) \quad (36)$$

$$\tau_{xz}^*(x^*, y^*, 0, \tau) = 0 \quad (37)$$

$$\tau_{yz}^*(x^*, y^*, 0, \tau) = 0 \quad (38)$$

$$\Pi(y^*) u_z^*(x^*, 0, 0, \tau) = u_B^*(x^*, \tau), \quad |y^*| \leq L_{Bal}^* \quad (39)$$

式中: $q_z^*(x^*, \tau) = q_z(x^*, \tau)/\mu$ 为土体受到道砟层的无量纲作用力; $u_B^*(x^*, \tau) = u_B(x^*, \tau)/a$ 为道砟

层底部与土体接触面的无量纲位移; $h^* = h/a$ 为无量纲加筋层厚度。

荷载分布函数的表达式为:

$$\Pi(y^*) = \begin{cases} 1 & |y^*| \leq L_{Bal}^* \\ 0 & |y^*| > L_{Bal}^* \end{cases} \quad (40)$$

式中, $L_{Bal}^* = L_{Bal}/a$, a 为无量纲道砟层宽度的一半。

加筋路堤层与饱和半空间之间的边界条件为:

$$u^*(x^*, y^*, h^*, \tau) = u_x^*(x^*, y^*, h^*, \tau) \quad (41)$$

$$v^*(x^*, y^*, h^*, \tau) = u_y^*(x^*, y^*, h^*, \tau) \quad (42)$$

$$w^*(x^*, y^*, h^*, \tau) = u_z^*(x^*, y^*, h^*, \tau) \quad (43)$$

$$\sigma_{zz}^*(x^*, y^*, h^*, \tau) = \sigma_{0zz}^*(x^*, y^*, h^*, \tau) \quad (44)$$

$$\tau_{xz}^*(x^*, y^*, h^*, \tau) = \tau_{0xz}^*(x^*, y^*, h^*, \tau) \quad (45)$$

$$\tau_{yz}^*(x^*, y^*, h^*, \tau) = \tau_{0yz}^*(x^*, y^*, h^*, \tau) \quad (46)$$

$$p^*(x^*, y^*, h^*, \tau) = 0 \quad (47)$$

应用式(36)~(38)和式(41)~(47)所示的边界条件解得 A_k, B_k, C_k 及 A~D 的表达式,则土体表面位移的表达式为:

$$\bar{u}_z^*(\xi, \eta, \Omega) = \bar{q}_z(\xi, \Omega) \Psi(\xi, \eta, \Omega) \quad (48)$$

式中, $\Psi(\xi, \eta, \Omega) = -\frac{1}{2a} \bar{\Pi}(\eta) \sum_{k=1}^6 C_k$

采用的轨道系统模型中将钢轨简化为无限长弹性 Euler 梁。无量纲 Euler 梁的动力方程为:

$$\delta \frac{\partial^4 u_R^*(x^*, \tau)}{\partial x^{*4}} + m_R^* \frac{\partial^2 u_R^*(x^*, \tau)}{\partial \tau^2} + k_P^* [u_R^*(x^*, \tau) - u_S^*(x^*, \tau)] = \begin{cases} F_z^*(x^*, \tau) & x^* - c^* \tau = 0 \\ 0 & x^* - c^* \tau \neq 0 \end{cases} \quad (49)$$

式中: $u_R^* = u_R/a$ 为 Euler 梁无量纲竖向变形; $\delta = EI/\mu a^4$ 为无量纲钢轨刚度; $m_R^* = m_R/\rho a^2$ 为钢轨单位长度无量纲质量; $k_P^* = k_P/\mu a$ 为钢轨与枕木之间弹簧的无量纲弹性常数; $F_z^* = F_z/\mu a^2$ 为钢轨所受的无量纲荷载; u_S^* 为枕木的无量纲竖向变形; $c^* = V \sqrt{\rho/\mu}$ 为无量纲荷载移动速度; $x^* - c^* \tau$ 为荷载作用点。

将枕木模拟成连续质量块,但不考虑其弯曲情况,故可将梁视为刚体。枕木的动力方程如下:

$$m_S^* \frac{\partial^2 u_S^*(x^*, \tau)}{\partial \tau^2} + k_P^* [u_S^*(x^*, \tau) - u_R^*(x^*, \tau)] = -F_S^*(x^*, \tau) \quad (50)$$

式中: $m_S^* = m_S/\rho a^2$ 为单位长度枕木的无量纲质量; $F_S^* = F_S/\mu a^2$ 为枕木与道砟层之间的无量纲相互作用力。

道砟层采用 Suiker^[18] 提出的 Cosserat 模型。道砟被简化为宽度为 $2a$ 的黏弹性层,单位长度质量

m_B , 该道砟层只考虑垂直刚度 k_B , 可推导得到道砟层顶部与底部的无量纲动力方程如下:

$$\begin{aligned} & \frac{m_B^*}{6} \left[2 \frac{\partial^2 u_S^*(x^*, \tau)}{\partial \tau^2} + \frac{\partial^2 u_B^*(x^*, \tau)}{\partial \tau^2} \right] + \\ & k_B^* [u_S^*(x^*, \tau) - u_B^*(x^*, \tau)] = F_S^*(x^*, \tau) \quad (51) \\ & \frac{m_B^*}{6} \left[\frac{\partial^2 u_S^*(x^*, \tau)}{\partial \tau^2} + 2 \frac{\partial^2 u_B^*(x^*, \tau)}{\partial \tau^2} \right] + \\ & k_B^* [-u_S^*(x^*, \tau) + u_B^*(x^*, \tau)] = -F_B^*(x^*, \tau) \quad (52) \end{aligned}$$

式中: $m_B^* = m_B/\rho a^2$ 为单位长度道砟层无量纲质量; $k_B^* = k_B/\mu a$ 为道砟层与枕木之间的无量纲弹簧常数; $F_B^* = F_B/\mu a^2$ 为土体与道砟层之间的无量纲相互作用力, 且 $F_B^* = 2a \cdot q_z^*(x^*, \tau)$ 。

对式(49)~(52)进行 τ, x, y 的三重 Fourier 变换, 消去 F_S^* 得如下变换域内轨道系统的动力方程组:

$$\bar{F}_B^*(\xi, \Omega) = \frac{\alpha_2(\xi, \Omega)\alpha_4(\xi, \Omega)k_P^*}{\alpha_1(\xi, \Omega)\alpha_6(\xi, \Omega)\alpha_4^2(\xi, \Omega) - (\alpha_3(\xi, \Omega) \cdot \alpha_1(\xi, \Omega) - k_P^{*2})(1 + \alpha_5(\xi, \Omega)\alpha_6(\xi, \Omega))} \quad (54)$$

则 Fourier 变换域内加筋土体的竖向变形表达式为:

$$\bar{u}_z^*(\xi, \eta, z^*, \Omega) = -\bar{\Pi}(\eta) \bar{F}_B^*(\xi, \Omega) \varphi(\xi, \eta, z^*, \Omega) \quad (55)$$

钢轨竖向变形表达式为:

$$\bar{u}_R^*(\xi, \Omega) = \frac{-(\alpha_2(\xi, \Omega)\alpha_4(\xi, \Omega)^2 - \alpha_2(\xi, \Omega)\alpha_3(\xi, \Omega) \cdot \alpha_5(\xi, \Omega) - \alpha_4(\xi, \Omega)\bar{F}_B^*(\xi, \Omega)k_P^*)}{(\alpha_1(\xi, \Omega)\alpha_4(\xi, \Omega)^2 - \alpha_1(\xi, \Omega)\alpha_3(\xi, \Omega) \cdot \alpha_5(\xi, \Omega) + \alpha_5(\xi, \Omega)k_P^{*2})} \quad (56)$$

引入移动坐标轴 $x_i^* = x^* - c^* \tau$, 则加筋土体竖向变形的时域表达式为:

$$u_z^*(x_i^*, y^*, z^*) = \frac{1}{4\pi^2} \int_{-\infty}^{\infty} \int_{-\infty}^{\infty} -\bar{\Pi}(\eta) \bar{F}_B^*(\xi, -\xi c^*) \cdot \varphi(\xi, \eta, z^*, -\xi c^*) e^{i[\xi x_i^* + \eta y^*]} d\xi d\eta \quad (57)$$

钢轨竖向变形的时域表达式为:

$$u_R^*(x^*, \tau) = \frac{1}{2\pi} \int_{-\infty}^{\infty} \bar{u}_R^*(\xi, -\xi c^*) e^{i\xi(x^* - c^* \tau)} d\xi \quad (58)$$

2 数值计算及讨论

采用 Fast Fourier Transform (FFT) 来计算 Fourier 逆变换。为确保 FFT 法计算所得的 Fourier 逆变换结果足够精确, 根据文献^[10]将 $-4 < \xi < 4$ 和 $-4 < \eta' < 4$ 的区间分割成 1024×1024 个区间进行计算。土体 Lamé 常数为: $\lambda^* = \lambda(1 + 2i\beta)$, $\mu^* = \mu(1 + 2i\beta)$, 其中 β 为材料阻尼比。

列车参数、饱和半空间土体和轨道系统的计算参数取自文献^[10, 12], 见表 1 和表 2。其中假设液相黏度为常数, 因此 b^* 的变化代表土体渗透系数的变

$$\left. \begin{aligned} & \alpha_1(\xi, \Omega) \bar{u}_R^*(\xi, \Omega) - k_P^* \bar{u}_S^*(\xi, \Omega) = \alpha_2(\xi, \Omega) \\ & -k_P^* \bar{u}_R^*(\xi, \Omega) + \alpha_3(\xi, \Omega) \bar{u}_S^*(\xi, \Omega) + \alpha_4(\xi, \Omega) \bar{u}_B^*(\xi, \Omega) = 0 \\ & \alpha_4(\xi, \Omega) \bar{u}_S^*(\xi, \Omega) + \alpha_5(\xi, \Omega) \bar{u}_B^*(\xi, \Omega) = -\bar{F}_B^*(\xi, \Omega) \\ & \bar{u}_B^*(\xi, \Omega) = \alpha_6(\xi, \Omega) \bar{F}_B^*(\xi, \Omega) \end{aligned} \right\} \quad (53)$$

式中:

$$\begin{aligned} \alpha_1(\xi, \Omega) &= \delta \xi^4 - m_B^* \Omega^2 + k_P^* \\ \alpha_2(\xi, \Omega) &= F_z^*(\xi, \Omega) \\ \alpha_3(\xi, \Omega) &= -m_B^* \Omega^2 / 2 + k_P^* + k_B^* - m_S^* \Omega^2 \\ \alpha_4(\xi, \Omega) &= -m_B^* \Omega^2 / 6 - k_B^* \\ \alpha_5(\xi, \Omega) &= -m_B^* \Omega^2 / 3 + k_B^* \\ \alpha_6(\xi, \Omega) &= \Psi(\xi, 0, \Omega) \end{aligned}$$

$\Psi(\xi, 0, \Omega) = \frac{1}{2\pi} \int_{-\infty}^{\infty} -\bar{\Pi}(\eta) \varphi(\xi, \eta, 0, \Omega) e^{i\eta y^*} dy^*$ 由式(53)解得关于加筋土体与道砟层之间作用力的表达式为:

化。当 $b^* = 0.1$ 时, 代表渗透系数较大的土体, 例如砂土; 当 $b^* = 100$ 时, 代表渗透系数较小的土体, 例如黏土。

表 1 土体及轨道系统参数

无量纲参数	数值
液相模量 M^*	12
液相密度 ρ^*	0.53
Lamé 常数 λ^*	2
土体阻尼比 β	0.02
土体结构参数	1.562 5
土颗粒压缩性系数 α	0.97
液相黏滞系数与土体渗透系数之比 b^*	10
道砟层宽度 L^*_{Bal}	2
钢轨刚度 δ	1
弹簧常数 $k_P^* = k_B^*$	2.7
单位长钢轨质量 m_R^*	2
单位长枕木质量 m_S^*	4
单位长道砟层质量 m_B^*	10

表 2 列车参数

L_{Eng}^*	L_{Wag}^*	L_{Dis}^*	P_{Eng}^*	P_{Wag}^*	a_t^*	b_t^*	d_t^*
22.2	24.4	-35	0.008	0.005	2.9	14.8	4

为了验证轨道模型及结果的准确性,当加筋率 $\eta = 0$ 时,假设本文中枕木与道砟层之间的弹簧常数为 0,将本文计算模型退化为文献^[10]的计算模型,并引入空间辅助坐标 $x_t^* = x^* - c\tau$,将计算结果与该文结果进行了对比,如图 2 所示。由图可见,计算结果与文献^[10]中所得结果吻合较好,从而验证了本文计算模型的正确性。

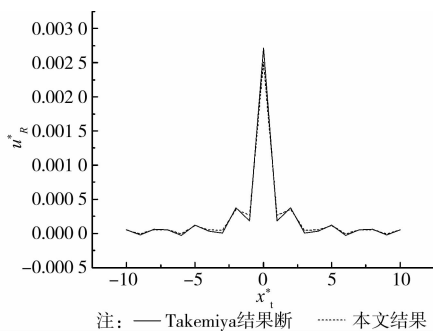


图 2 本文结果与文献[10]对比

图 3 给出了不同加筋率情况下,速度对钢轨竖向变形的影响。钢轨竖向变形随着速度的增大而增大,在速度达到一定值后,钢轨竖向变形开始呈现下降趋势。这可能与土体 Rayleigh 波速的大小有关,当荷载移动速度接近土体的 Rayleigh 波速时,轨道系统和土体将产生共振,此时竖向变形最大;之后竖向变形随荷载增大而减小。垫层填土采用砂土,当路堤厚度相同时,加筋路堤上钢轨竖向变形比不加筋 ($\eta = 0$) 路堤上的钢轨竖向变形要小,说明加筋后路堤的刚度增大,从而减小了钢轨的竖向变形;同时,在加筋率由 0.01 增大到 0.025 过程中。随着加筋率的增大,钢轨竖向变形呈现递减趋势,例如 $c^* = 0.8, \eta = 0.01$ 时钢轨的竖向变形为 0.003 6; $c^* = 0.8, \eta = 0.025$ 时钢轨的竖向变形为 0.003 4,变形值减小了 6%。

图 4 给出了相同垫层厚度下荷载幅值大小对钢轨竖向变形的影响,在 $x_t^* = 0$ 附近,钢轨竖向变形随着荷载幅值的增大呈现明显的增大趋势,随着距观察点 ($x_t^* = 0$) 的增大,钢轨竖向变形逐渐减小。加筋率同为 0.02 时,无量纲荷载幅值 $Q^* = 0.2$ 时的钢轨竖向变形为 0.002, $Q^* = 0.4$ 时为 0.007,后者比前者增加了 2.5 倍。在无量纲荷载幅值 $Q^* = 0.2$ 时, $x_t^* = 0$ 处,加筋路堤上钢轨竖向变形为

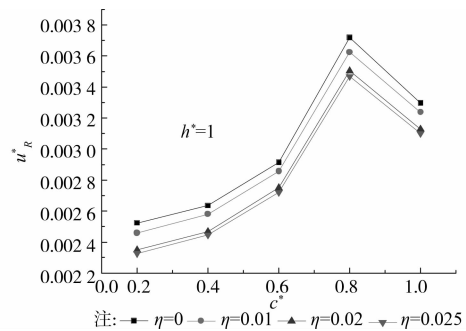


图 3 速度对钢轨竖向变形的影响

0.002,而未加筋路堤上钢轨竖向变形约为 0.004 5,竖向变形约降低了 55%;当无量纲荷载幅值 $Q^* = 0.4$ 时, $x_t^* = 0$ 处,加筋路堤上钢轨变形 0.007,未加筋情况下,钢轨的变形则 0.009,竖向变形约降低了 22%。由上可知,在荷载幅值和路堤厚度相同的情况下,加筋路堤上钢轨变形远小于未加筋路堤上钢轨竖向变形。

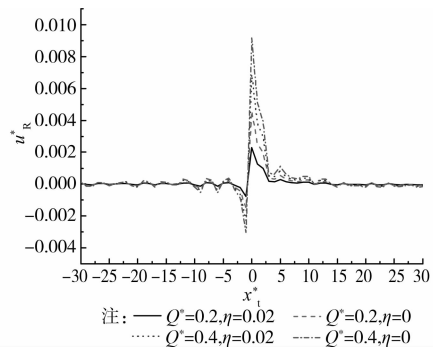


图 4 荷载幅值大小对钢轨竖向变形影响

图 5 给出了不同速度下,加筋率 $\eta = 0.02$ 时,加筋路堤厚度对钢轨竖向变形的影响。钢轨变形随着加筋土层厚度的增加整体上呈现减小趋势,当 h^* 大于 4 后,加筋垫层厚度对钢轨竖向变形的影响不再明显。同时,同一垫层厚度且加筋率相同的情况下,随着速度的增大,钢轨竖向变形也呈现增大趋势。

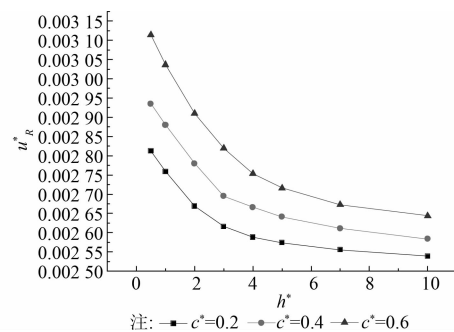


图 5 加筋层厚度对钢轨竖向变形的影响

图 6 给出了加筋垫层的加筋率对钢轨竖向变形

的影响;随着加筋率的增大,钢轨竖向变形呈现减小趋势。当加筋率在 0.010~0.020 范围内时,钢轨变形的减小率($\Delta\mu/\Delta\eta$)较大,加筋效果较为明显;当加筋率大于 0.022 5 后,钢轨变形变化不大,趋向于一条水平线,表明此后的加筋效果不明显。同时,在加筋率相同的情况下,钢轨变形随加筋垫层厚度的增大而呈现减小趋势。

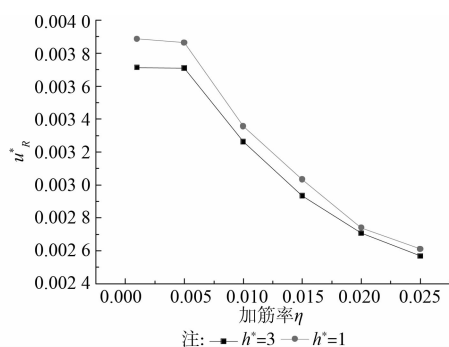


图 6 加筋率对钢轨竖向变形的影响

3 结 论

采用解析法研究了移动荷载作用下,下卧饱和土体上加筋路堤及其上轨道系统的三维动力响应问题。研究了列车移动速度、加筋垫层的厚度、荷载幅值大小和加筋率等对轨道系统动力响应的影响。

1) 钢轨竖向变形随着速度的增大而增大;在速度达到一定值后,钢轨竖向变形随速度增大呈现下降趋势。路堤厚度相同时,作用于加筋路堤上钢轨的竖向变形明显小于不加筋路堤的情况。

2) 路堤厚度相同时,观察点附近,钢轨的竖向变形随着荷载幅值的增大呈现显著的增大趋势。

3) 随着加筋率的增大,钢轨竖向变形呈现减小趋势;在加筋率相同的情况下,钢轨变形随加筋路堤厚度的增大而呈现减小趋势。

参考文献:

[1] Wang L P, Zhang G, Zhang J M. Centrifuge model tests of geotextile-reinforced soil embankments during an earthquake [J]. *Geotextiles and Geomembranes*, 2011, 29(3): 222-32.

[2] Nazzal M D, Abu-Farsakh M Y, Mohammad L N. Implementation of a critical state two-surface Model to evaluate the response of geosynthetic reinforced pavements[J]. *International Journal of Geomechanics*, 2010, 10(5): 202-212.

[3] Kwon J, Tutumluer E, Al-Qadi I L. Validated mechanistic model for geogrid base reinforced flexible pavements[J]. *Journal of Transportation Engineering*,

2009, 135(12):915-926.

- [4] Huang X M, Wang H. Comparison between responses of reinforced and unreinforced embankments due to road widening[J]. *Journal of Central South University of Technology*, 2009, 16: 857-864.
- [5] Maheshwari P, Viladkar M N. A mathematical model for beams on geosynthetic reinforced earth beds under strip loading [J]. *Applied Mathematical Modelling*, 2009, 33: 1803-1814.
- [6] 刘飞禹, 赵国兴, 蔡袁强, 等. 移动荷载下加筋道路系统的动力响应 [J]. *浙江大学学报:工学版*, 2007, 41(1): 57-65.
Liu F Y, Zhao G X, Cai Y Q, et al. Dynamic response of reinforced pavements system subjected to moving loads[J]. *Journal of Zhejiang University: Engineering Science*, 2007, 41(1): 57-65.
- [7] Saad B, Mitri H, Poorooshasb H. 3D FE analysis of flexible pavement with geosynthetic reinforcement [J]. *Journal of Transportation Engineering*, 2006, 132(5): 402-415.
- [8] Maheshwari P. Analysis of rails on damped tensionless reinforced earth beds under moving loads [J]. *International Journal of Geotechnical Engineering*, 2010, 4(1): 127-137.
- [9] 李西斌, 吴金耀, 齐 锋. 高速列车荷载下桩承加筋路堤荷载传递机制数值分析[J]. *土木工程学报*, 2011, 44: 55-60.
Li X B, Wu J R, Qi F. Stress transfer mechanism of geosynthetic reinforced pile supported embankment due to high-speed train loading[J]. *China Civil Engineering Journal*, 2011, 44: 55-60.
- [10] Takemiya H, Bian X C. Substructure simulation of inhomogeneous track and layered ground dynamic interaction under train passage [J]. *Journal of Engineering Mechanics, ASCE*, 2005, 131(7): 699-711.
- [11] Maheshwari P, Viladkar M N. Soil-structure interaction of damped infinite beams on extensible geosynthetic reinforced earth beds under moving loads [J]. *Geotechnical and Geological Engineering*, 2010, 28(5): 579-590.
- [12] Sun H L, Cai Y Q, Xu C J. Three-dimensional steady-state response of a railway system on layered half-space soil medium subjected to a moving train [J]. *International Journal for Numerical and Analytical Methods in Geomechanics*, 2009, 33: 529-550.
- [13] Xu B, Lu J F, Wang J H. Dynamic response of an infinite beam overlying a layered poro-elastic half-space to moving loads [J]. *Journal of Sound and Vibration*, 2007, 306: 91-110.

(下转第 120 页)

Cement Products, 2009(4): 41-44.

- [15] Vancura M, MacDonald K, Khazanovich L. Structural analysis of pervious concrete pavement [J]. Transportation Research Record, 2011, 2226: 13-20.
- [16] Goede W, Haselbach L. Investigation into the structural performance of pervious concrete [J]. Journal of Transportation Engineering, 2011, 138(1): 98-104.
- [17] 杨志峰. 多孔混凝土透水基层材料组成设计与性能研究 [D]. 武汉: 武汉理工大学, 2008.
- [18] 中华人民共和国行业标准. 普通混凝土力学性能试验方法标准 GB/T 50081-2002[S]. 北京: 人民交通出版社, 2002.
- [19] 周剑平. Origin 实用教程 7.5[M]. 西安: 西安交通大学出版社, 2007.
- [20] 崔新壮, 王聪, 周亚旭, 等. 透水性混凝土桩减压减震耦合抗震机理研究[J]. 山东大学学报: 工学版, 2012, 42(4): 86-91.
- Cui X Z, Wang C, Zhou Y X, et al. Anti-earthquake mechanism of pervious concrete pile composite foundation [J]. Journal of Shandong University: Engineering Science, 2012, 42(4): 86-91.

(编辑 薛婧媛)

(上接第 108 页)

- [14] Xu B, Lu J F, Wang J H. Dynamic response of a layered water-saturated half-space to a moving load [J]. Computer and Geotechnics, 2008, 35:1-10.
- [15] Biot M A. Mechanics of deformation and acoustic propagation in porous media [J]. Journal of Applied Physics, 1962, 33:1482-1498.
- [16] Chen T C, Chen R H, San-shyan L. A nonlinear homogenized model applicable to reinforced soil analysis [J]. Geotextiles and Geomembranes, 2000, 18(6): 349-366.
- [17] Michalowski R L, Zhao A. Continuum versus structural approach to stability of reinforced soil [J]. Journal of Geotechnical Engineering, ASCE, 1995, 121(2): 152-162.
- [18] Suiker A S J. Surface waves in a stratified half space with enhanced continuum properties. Part 1: Formulation of the boundary value problem [J]. European Journal of Mechanics A: Solids, 1999, 18:749-768.

(编辑 胡玲)